Food Chemistry: X 23 (2024) 101671

Contents lists available at ScienceDirect

Food Chemistry: X

journal homepage: www.sciencedirect.com/journal/food-chemistry-x

# Purification, characterization, simulated gastrointestinal digestion and gut microbiota fermentation of a *Bifidobacterium*-directed mannoglucan from *Lilium brownii* var. *viridulum*

Guangjian Bai [a,b], Miaoyun Ye [a], Li Yu [a], Ming Yang [a], Yaqi Wang [a,*], Shaodan Chen [b,*]

[a] Key Laboratory of Modern Preparation of TCM, Ministry of Education, Jiangxi University of Chinese Medicine, Nanchang 330004, China
[b] National Health Commission Science and Technology Innovation Platform for Nutrition and Safety of Microbial Food, Guangdong Provincial Key Laboratory of Microbial Safety and Health, State Key Laboratory of Applied Microbiology Southern China, Institute of Microbiology, Guangdong Academy of Sciences, Guangzhou 510070, China

ARTICLE INFO

*Keywords:*
*Lilium brownii* var. *viridulum*
*Bifidobacterium*-directed polysaccharides
Mannoglucan
Gut microbiota
Acetic acid

ABSTRACT

*Lilium brownii* var. *viridulum* (Longya lily) is an edible vegetable and medicinal plant with the effects of moistening lungs, relieving coughs, and removing phlegm. In this study, a homogenous mannoglucan LLP11 was purified from Longya lily using membrane ultrafiltration followed by ion exchange chromatography. The $M_w$ of LLP11 was 12.0 kDa. LLP11 exhibited a backbone of →4)-α-D-Glc*p*-(1 → and →4)-β-D-Man*p*-(1 → with a branch of T-α-D-Glc*p*-(1 → substituted at C-6 of →4,6)-α-D-Glc*p*-(1→. During the simulated digestion, LLP11 remained indigestible to digestive enzymes. Furthermore, through its interaction with the gut microbiota, LLP11 was able to significantly boost *Bifidobacterium* and decrease the harmful bacteria *Klebsiella*, that was linked to pneumonia. Additionally, LLP11 promoted the growth of *B. pseudocatenulatum* and *B. longum* and was utilized to produce acetic acid. Our findings introduced an alternative approach for the investigation of microbiota-targeted polysaccharides and underscored the potential of LLP11 as a prebiotic for supplementary treatment in respiratory diseases.

## 1. Introduction

The human intestinal tract harbors hundreds of trillions of microorganisms including bacteria, viruses, archaea, and eukaryotes. Collectively, these microorganisms form a complex microbial ecosystem that establishes a mutually symbiotic relationship with the host (Liu et al., 2021). The imbalance of the gut microbiota (GM) such as an overproliferation of pathogenic bacteria or a substantial reduction in beneficial bacteria will contribute to systemic diseases (Vujkovic-Cvijin et al., 2020). Thus, maintaining a balance of GM is vital for human wellness.

Food-derived polysaccharides are becoming increasingly well-known due to their wide range of biological activities, which are both highly effective and lowly toxic. Due to the high molecular weight ($M_w$) and low liposolubility, most polysaccharides, in contrast to small molecules, are complicated for the upper gastrointestinal tract to digest directly (Bai et al., 2023; Li et al., 2020). Bioactive polysaccharides serve as prebiotics to benefit host health by inhibiting harmful intestinal bacteria and promoting beneficial bacteria (Bai et al., 2023). More importantly, increasing research further supported that polysaccharides were degraded into applicable oligosaccharides/monosaccharides and other metabolites such as short-chain fatty acids (SCFAs) by carbohydrate-active enzymes (CAZymes) which are explicitly encoded by GM (Feng et al., 2019; Zhang et al., 2022). The dynamic balance of GM combined with the metabolites of polysaccharides exerts beneficial physiological regulatory effects on the host including pathogen defense, inflammation inhibition, and metabolism regulation (Bai, Zhou, Zhang, et al., 2023). The cross-interaction of polysaccharides, GM, and correlated diseases has become a research hotspot.

*Lilium brownii* var. *viridulum*, with the local name of Longya lily, is an edible plant with high ornamental, valuable nutritional, and medicinal properties. The bulb of lily is sweet and delicious, which is attributed to its nutritional ingredients such as starch, polysaccharide, protein, fat, etc. (Li et al., 2020). Lily is not only a highly valued culinary element but is also said to have ancient Chinese medicinal properties. It has been

* Corresponding author at: State Key Laboratory of Applied Microbiology Southern China, Institute of Microbiology, Guangdong Academy of Sciences, No. 100 Xianlie.
*E-mail addresses:* wangyaqi_3@163.com (Y. Wang), shaodanchen@126.com (S. Chen).

https://doi.org/10.1016/j.fochx.2024.101671
Received 27 September 2023; Received in revised form 26 February 2024; Accepted 16 July 2024
Available online 18 July 2024

recorded in "Chinese Pharmacopoeia" for its effects of moistening lungs, relieving coughs, and removing phlegm (Zhu, Luo, Lv, & Kong, 2014). Modern pharmacology research has found that *Lilium* has the effects of anti-tumor, immunomodulation, antioxidant, and intestinal microflora regulation (Zhou, An, & Huang, 2021). Polysaccharides may be one of the most important contributors to such medicinal properties. Phytochemical research has found that *Lilium* polysaccharides mainly contain glucans or glucomannans, whose backbone have the residues of →4)-α-Glc*p*- (1→, →6)-α-Glc*p*- (1→, →4)-β-Glc*p*- (1→, →6)-β-Glc*p*- (1→, →4)-α-Man*p*- (1→, →3)-β-Man*p*- (1 → and →4)-β-Man*p*- (1 → (Li et al., 2020; Wang, Wang, Niu, Huang, & Zhang, 2018; Zhang et al., 2022; Zhang, Gao, Zhou, Hu, & Xie, 2010). However, the structural characteristics of Longya lily polysaccharides, as well as the interaction between bioactive Longya lily polysaccharides and GM remain unclear.

In this study, a novel mannoglucan LLP11, was isolated and purified from Longya lily using membrane ultrafiltration followed by ion exchange chromatography. It is worth mentioning that membrane ultrafiltration combined with ion exchange chromatography technology is a highly efficient method for polysaccharide classification. A comprehensive evaluation of LLP11 from simulated digestion, gut microbiota fermentation, and bioactivity on probiotic strains *in vitro* was further carried out. This work can contribute to exploring microbiota-directed polysaccharides from edible or medicinal plants, and providing a shred of evidence to understand the polysaccharides in prebiotic applications.

## 2. Materials and methods

### 2.1. Materials and chemicals

The bulbs of Longya lily were provided by Jiangxi Jiangzhong Chinese Herbal Pieces Co., Ltd., and identified as *Lilium brownii* var. *viridulum* Baker by Prof. Ming Yang (Jiangxi University of Chinese Medicine, Nanchang, China). Monosaccharides standards were obtained from Yuanye Bio-Technology Co., Ltd. (Shanghai, China). Dextran standards ($M_w$: 2–670 kDa) were from Sigma (St. Louis, USA).

### 2.2. Extraction and purification of LLP11 from Longya lily

Dried bulbs of Longya lily (1 kg) were soaked in 95% ethanol overnight to remove the lipophilic compounds. The solvent-evaporating residues were extracted with distilled water (1:12, *w/v*), which includes pectinase (3%, *w/w*) and papain (1%, *w/w*). The mixture is maintained at 50 °C for 1 h, then heated up to 70 °C for another 1 h, and finally, boiled for 5 min to inactivate the enzymes. The extraction procedure was repeated three times. The extraction solution was concentrated, centrifuged, and treated with 80% ethanol precipitation. The precipitate was collected and freeze-dried to obtain Longya lily crude polysaccharide extract (LLP). LLP (6 g) was dissolved in 1.0 L of distilled water and filtered through a 0.22 μm microporous membrane. The filtrate was subjected to an ultrafiltration membrane ($M_W$10 kDa, Vivaflow 200, Sartorius, Germany), and the percolate with $M_w > 10$ kDa was collected and named LLP1. LLP1 was then purified on a DEAE Sepharose™ Fast Flow column (Cytiva, Danderyd, Sweden) and eluted stepwise with water, followed by 0.1 M and 0.5 M sodium chloride solutions based on preliminary experiments. A prominent peak from water elution was picked up based on the curve drawn by the phenol-sulfuric acid reaction. After being concentrated and freeze-dried, LLP11 was obtained.

### 2.3. Homogeneity and $M_w$ determination

HPGPC determined the homogeneity and $M_w$ of LLP11 on a Shimadzu SIL-20A HPLC system equipped with a RID-20A RI detector and GPC software (Shimadzu, Japan) based on the reported method (Gao et al., 2022).

### 2.4. Chemical composition analysis

The total carbohydrate content of LLP11 was measured by the phenol-sulfuric acid method (Dubois, Gilles, Hamilton, Rebers, & Smith, 1951). The total protein was quantified by a BCA protein assay kit.

### 2.5. Monosaccharide composition identification

LLP11 was fully acid hydrolyzed as described previously (Chen, Zhang, Zhu, Yang, & Han, 2014). The hydrolysate and mixed monosaccharide standards were respectively analyzed using a Dionex ICS-6000 HPAEC-PAD system (Thermo Scientific, USA) equipped with a Dionex Carbopac™ PA20 column (3 × 150 nm, Thermo Scientific, USA).

### 2.6. Methylation analysis

LLP11 was subjected to complete methylation and hydrolysis successively as in our previous report (Chen et al., 2022). The hydrolysate was then prepared into partially methylated alditol acetates (PMAA), which were then analyzed by GC–MS. The stepped temperature program was initially set at 120 °C, then increased to 250 °C at 3 °C/min and held for 5 min. The FID and injection temperature was 250 °C.

### 2.7. FT-IR and NMR analysis

FT-IR spectrum was acquired on a Bruker FT-IR spectrophotometer II after preparing the KBr pellet mixed with dried LLP11.

Dried powder of LLP11 (30 mg) was dissolved in 0.5 mL of $D_2O$ and centrifuged. The supernatant was transferred to an NMR tube and mixed with 20 μL of deuterated acetone ($\delta_H = 2.05$ ppm and $\delta_C = 29.7$ ppm). The NMR spectra were obtained from a Bruker Advance III HD 600 NMR spectrometer at 25 °C.

### 2.8. Simulated digestion of LLP11

The *in vitro* simulated digestion including simulated saliva fluid (SSF), gastric fluid (SGF), and intestinal fluid (SIF) digestion was carried out as described by Fu et al. (2023) with slight modifications. LLP11 solution (4 mL, 10 mg/mL) mixing with 4 mL of SSF (containing α-amylase) was set as the experimental group. Similarly, an equal volume of LLP11 solution added to deionized water was set as the control group, and 4 mL of SSF with 4 mL of deionized water was the blank group. All the samples were incubated at 37 °C for 2 min. An equal volume of 2 mL from the digestive solution was taken out at 0 and 2 min for enzyme inactivation.

After saliva digestion, the experimental and blank groups were added with SGF (Solarbio, Beijing, China) to reach a volume of 8 mL, respectively. In contrast, the control group was added with the same amount of deionized water. All the samples were incubated at 37 °C. Equal parts of the digestive solution (2 mL) were drawn, and enzymes were inactivated at 0, 1, and 2 h. Lastly, 3 mL of SIF (Solarbio, Beijing, China) was added to the SSF and SGF digestion juice. Again, the control group was added with the same amount of deionized water and incubated at 37 °C. The digestion juice was taken out and enzymes were inactivated at 0, 1, 2, and 4 h.

### 2.9. Fecal fermentation in vitro

The fermentation of LLP11 is based on a previous method with slight adjustments (Tian et al., 2023). LLP11 (10 mg/mL) was dissolved into the essential nutrient medium (the formula is shown in Table S1). Feces were freshly collected from three healthy young volunteers (23–25 years old). Equivalent feces from each volunteer were thoroughly mixed and suspended into the essential medium (1:10, *w/v*) and centrifuged. An equal amount of the supernatant (0.5 mL) was transferred into a culture bottle. To this, 4.5 mL of LLP11-medium solution was added and the

mixture was anaerobically cultured at 37 °C. The group without LLP11 was marked as the blank control group (Con). After 24 h fermentation, the samples were quickly placed into liquid nitrogen to terminate fermentation, and transferred to −80 °C for preservation. The samples were dissolved on ice, centrifuged (8000 rpm, 4 °C, 10 min), and then packaged with the precipitation and supernatant for subsequent assays.

### 2.10. Analysis of gut microbiota

The total DNA of the fermented precipitation was extracted by a DNA extraction kit. Primers (341F as the upstream and 806R as the downstream primers) were used to amplify the sequence by polymerase chain reaction according to the V3 ~ V4 region. Sequencing was performed using the Illumina MiSeq platform, and analyzed through the Meji Biological cloud platform (www.cloud.majorbio.com).

### 2.11. SCFAs determination

Before SCFAs determination, the pH of the fermentation supernatant was assayed. Then, the SCFAs were extracted with ethyl acetate (repeated 3 times). The extracted solution was combined and dried under nitrogen. The dried extract was re-dissolved in ethyl acetate, filtered, and analyzed by GC. The temperature program was initially set at 65 °C and kept for 3 min, then increased to 200 °C at 45 °C/min and held for 2 min, and finally increased to 230 °C at 15 °C/min and kept for 2 min.

### 2.12. Bifidobacterium growth with LLP11 in vitro

*B. pseudocatenulatum* (BP, ATCC 27919) and *B. longum* (BL, ATCC 15707) were purchased from the American Type Culture Collection (ATCC). LLP11 was dissolved into the essential nutrient medium, and mixed with 10% bacteria solution (BP, BL, and mixed BP-BL) at a final concentration of 2.5, 5, and 10 mg/mL, respectively. An equal volume of BBL medium solution mixed with 10% bacteria solution were used as a control. The mixed solution was anaerobically cultured at 37 °C. Growth curves were plotted based on the $OD_{600}$ value of the fermentation liquor singly following 0, 12, 22, 30, 38, and 48 h.

### 2.13. Statistical analysis

Data were shown as mean ± standard deviation (SD). The statistically significant difference was calculated by one-way ANOVA followed by Tukey's test using SPSS (version 21.0) at a significance level of $\alpha = 0.05$.

## 3. Results and discussion

### 3.1. Separation and purification of LLP11

As shown in Fig. S1a-b, a homogenous polysaccharide LLP11 was separated and purified from LLP by membrane ultrafiltration followed by DEAE Sepharose Fast Flow column chromatography, which was eluted with distilled water. HPGPC analysis revealed a uniform symmetrical single peak for LLP11 with an $M_w$ of 12.0 kDa (as shown in Fig. S1c). The total carbohydrate content of LLP11 was 84.01 ± 0.1% and no protein was involved. The monosaccharide composition analysis (Fig. S1d) showed LLP11 contained glucose (89.79%) and mannose (10.21%).

### 3.2. FT-IR spectroscopy

The FT-IR spectrum (Fig. S2) of LLP11 showed characteristic peaks of a polysaccharide. The strong peak at 3422.5 $cm^{-1}$ was the stretching vibration of O—H, and the peak at 2930.3 $cm^{-1}$ represented the C—H stretching vibration (Wang et al., 2018). The absorption peak at 1638.2 $cm^{-1}$ was possibly due to bound water in polysaccharide hydrate (Zhang, Qin, et al., 2022). The near bands at 1415.0 and 1370.7 $cm^{-1}$ were attributed to the bending vibrations of -$CH_2$ and -CH-, respectively (Gao et al., 2022). Besides, the near peaks at 1153.2 and 1023.0 $cm^{-1}$ were related to the ring vibration of pyranose and C-O-C glycosidic bond vibration, respectively (Hui et al., 2019). Uppermost, both bands at 848.4 and 761.1 $cm^{-1}$ indicated the α-glycosidic linkages between the glycosidic residues (Gao et al., 2022).

### 3.3. Methylation analysis

As shown in Table S2, LLP11 contained T-Glc*p*-(1 → (7.46%), →4)-Glc*p*-(1 → (72.99%), →4,6)-Glc*p*-(1 → (7.58%) and →4)-Man*p*-(1 → (11.98%) based on the GC–MS analysis. The result of the glycosyl composition after methylation was in accordance with the monosaccharide composition.

### 3.4. NMR analysis

As shown in Fig. 1a, there were four anomeric proton peaks at $\delta_H$ 5.27, 5.26, 4.83, and 4.62 ppm in the $^1H$ NMR spectrum of LLP11. Correspondingly, four anomeric carbon signals at $\delta_C$ 100.12, 99.92, 99.78, and 98.78 ppm appeared in the $^{13}C$ NMR spectrum (Fig. 1b). Combining with the HSQC spectrum (Fig. 1c) and the glycosyl composition from GC–MS analysis, the signals at $\delta_H/\delta_C$ 5.27/99.78 and 5.26/99.92 were assigned as H-1/C-1 of →4)-α-D-Glc*p*-(1 → (residue **A**) and →4,6)-α-D-Glc*p*-(1 → (residue **B**), and $\delta_H/\delta_C$ 4.83/98.78 was assigned as H-1/C-1 of α-D-Glc*p*-(1 → (residue **C**). The weak signal at $\delta_H/\delta_C$ 4.62/100.12 was possibly ascribed to H-1/C-1 of →4)-β-D-Man*p*-(1 → (residue **D**). Besides, the down-fielded signal at $\delta_C$ 68.65 ppm in the $^{13}C$ NMR spectrum could be assigned to C-6 of →4,6)-α-D-Glc*p*-(1→. The signals at $\delta_C$ 60.65 and 60.59 ppm were scribed to C-6 of α-D-Glc*p*-(1 → and →4)-α-D-Glc*p*-(1→, respectively.

The assignments of H-2 ~ H-6 of each glycosidic residue could be determined from the signals of H-1 based on the $^1H$—$^1H$ COSY correlations (Fig. 1d). Taking →4)-α-D-Glc*p*-(1 → as an example, the chemical shifts of H-2 ~ H-6 were determined as $\delta_H$ 3.48, 3.84, 3.51, 3.71, and 3.69/3.72 based on the correlations of $\delta_H$ 5.27/3.48 (H1/H2), 3.48/3.84 (H2/H3), 3.84/3.51(H3/H4), 3.51/3.71 (H4/H5), 3.71/3.69 (H5/H6a), and 3.69/3.72 (H6a/H6b) in the $^1H$—$^1H$ COSY spectrum (Fig. 1d). Together with the HSQC correlation, the assignments of C-2 ~ C-6 of each glycosidic residue were also determined. The assignments of $^1H$ and $^{13}C$ NMR data (Table 1) were further confirmed by comparison with the reported data (Gao et al., 2022; Hou, Zhao, Yin, & Nie, 2023; Hui et al., 2019; Song et al., 2021).

In the HMBC spectrum (Fig. 1e), the apparent correlation peaks at 4.62/76.87 and 3.51/100.12 indicated that →4)-β-D-Man*p*-(1 → was connected to →4)-α-D-Glc*p*-(1→. The obvious correlation signals at 3.51/99.78 and 5.27/76.87 represented that →4)-α-D-Glc*p*-(1 → was neighbor to each other. The HMBC correlation between 5.27 and 77.15, as well as 3.54 and 99.78 indicated →4)-α-D-Glc*p*-(1 → was connected to →4,6)-α-D-Glc*p*-(1→. The cross peak at 3.72/98.78 manifested that T-α-D-Glc*p*-(1 → was linked at C-6 of →4,6)-α-D-Glc*p*-(1 → .

Thus, LLP11 was elucidated as a mannoglucan with a backbone consisting of →4)-α-D-Glc*p*-(1 → and →4)-β-D-Man*p*-(1→, with a branch of T-α-D-Glc*p* substituted at C-6 of →4,6)-α-D-Glc*p*-(1→. The repeating unit of LLP11 was shown in Fig. 1f.

### 3.5. Changes of LLP11 in the digestion of SSF, SGF, and SIF

Changes in the $M_w$ distribution can reflect the degradation and utilization of polysaccharides. As illustrated in Fig. 2a, the peak at 15.3 min represented the characteristic signal of LLP11. The HPGPC results at 0 and 2 min after SSF digestion almost overlapped, indicating that it was difficult for enzymes in saliva to hydrolyze LLP11. The robust acid environment of the stomach is where most food erosion occurs.

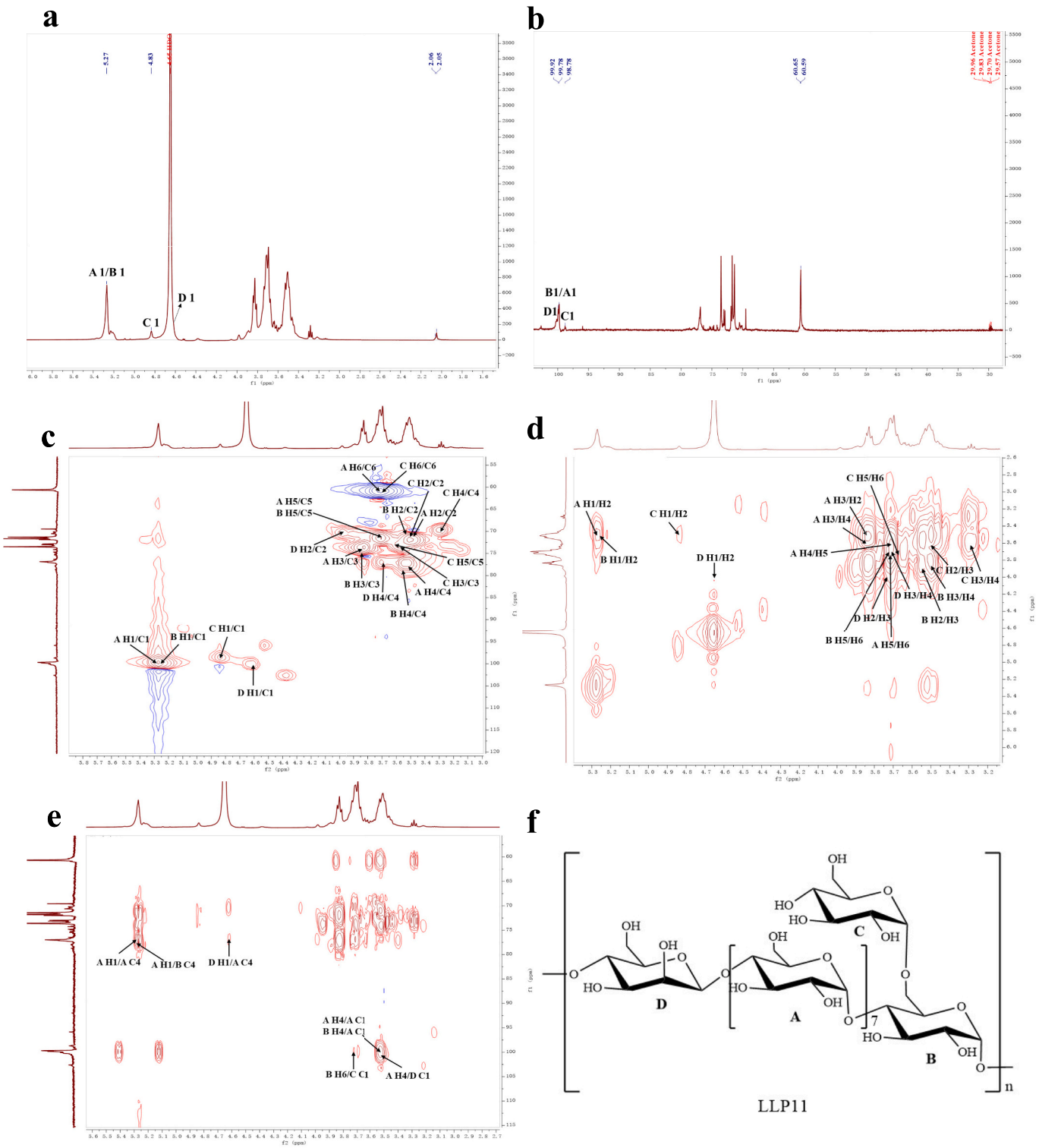


**Fig. 1.** NMR spectra (a-e) and the repeating unit (f) of LLP11.
$^{1}$H NMR (a), $^{13}$C NMR (b), HSQC (c), $^{1}$H—$^{1}$H COSY (d), HMBC (e), and the repeating unit of LLP11 (f).

However, as shown in Fig. 2b, no change occurred in the retention time of LLP11 during SGF digestion. The same result was also observed during SIF digestion (Fig. 2c), which indicated LLP11 was undegraded in the digestive tract.

The variation in reducing sugar and monosaccharides is also essential to assess the digestive characteristics of LLP11. The contents of reducing sugar of LLP11 in simulated digestive stages were presented in Fig. 2d-f. There was no difference in reducing sugar compared with 0 h. In addition, as depicted in Fig. 2g, the PMP-HPLC signals remained the same in each digestive stage. Although the glucose content in SGF significantly increased compared to that in SSF, there was no significant difference between 0, 1, and 2 h. This was due to the hydrolysis of LLP11 in conditions of strong acid and high temperature while preparing the analyte. Consequently, no monosaccharide was produced during the digestion.

**Table 1**
$^{1}$H and $^{13}$C NMR spectroscopic data of LLP11.

| Glycosyl residues | H1<br>C1 | H2<br>C2 | H3<br>C3 | H4<br>C4 | H5<br>C5 | H6<br>C6 |
|---|---|---|---|---|---|---|
| →4)-α-D-Glcp-(1 →<br>(A) | 5.27<br>99.78 | 3.48<br>71.72 | 3.84<br>73.56 | 3.51<br>76.87 | 3.71<br>71.30 | 3.69[a]/<br>3.72[b]<br>60.59 |
| →4,6)-α-D-Glcp-(1<br>→ (B) | 5.26<br>99.92 | 3.50<br>71.72 | 3.85<br>74.17 | 3.54<br>77.15 | 3.71<br>71.30 | 3.72<br>68.65 |
| α-D-Glcp-(1 → (C) | 4.83<br>98.78 | 3.49<br>71.90 | 3.60<br>73.02 | 3.28<br>69.49 | 3.64<br>72.85 | 3.67<br>60.65 |
| →4)-β-D-Manp-(1<br>→ (D) | 4.62<br>100.12 | 3.98<br>70.22 | 3.71<br>71.46 | 3.71<br>76.98 | ns<br>ns | ns<br>ns |

Note: "ns" means "no signal".

### 3.6. The effects of LLP11 on gut microbiota

The disturbance of GM is closely correlated with the occurrence and intervention of many diseases. On one hand, polysaccharides can act as probiotics, which regulate the microecological balance of GM. On the other hand, GM is also an active site for polysaccharides metabolism, which produces biological metabolites with potential health benefits (Wu et al., 2022).

The interaction between LLP11 and GM was carried out by fermentation *in vitro*. After 24 h fermentation, the total carbohydrate of LLP11 decreased by 30.1%, from 8.67 ± 0.05 to 6.06 ± 0.05 mg/mL. Besides, the peak area of LLP11 was reduced in HPGPC (Fig. S3), which indicated that GM utilized LLP11.

16S rRNA sequencing was then employed to analyze the effect of LLP11 on GM. Firstly, As shown in Fig. S4, the rarefaction curves gradually arrived at the plateau as the sequence numbers increased, which prompted that the acquired data was sufficient for further analysis. The Chao, Ace, and Shannon indexes were selected to evaluate the alpha diversity. The Chao and Ace indexes were used to estimate species richness, and the Shannon index reflected species diversity. As shown in Fig. S5a-c, no significant changes were observed in the values of the Chao, Ace, and Shannon indexes between the Con group and the LLP11 group, indicating that LLP11 maintained a good alpha diversity. The principal-coordinate analysis (PCoA) was used for estimating the beta diversity between the two groups. The result showed that a significant alteration occurred in the gut community composition structure after LLP11 treatment, as the cluster of LLP11 was far from that of the Con group (Fig. S5d). Then, bacterial populations between the Con group and the LLP11 group were compared. At the phylum level (Fig. 3a), LLP11 treatment significantly inhibited the abundance of Proteobacteria

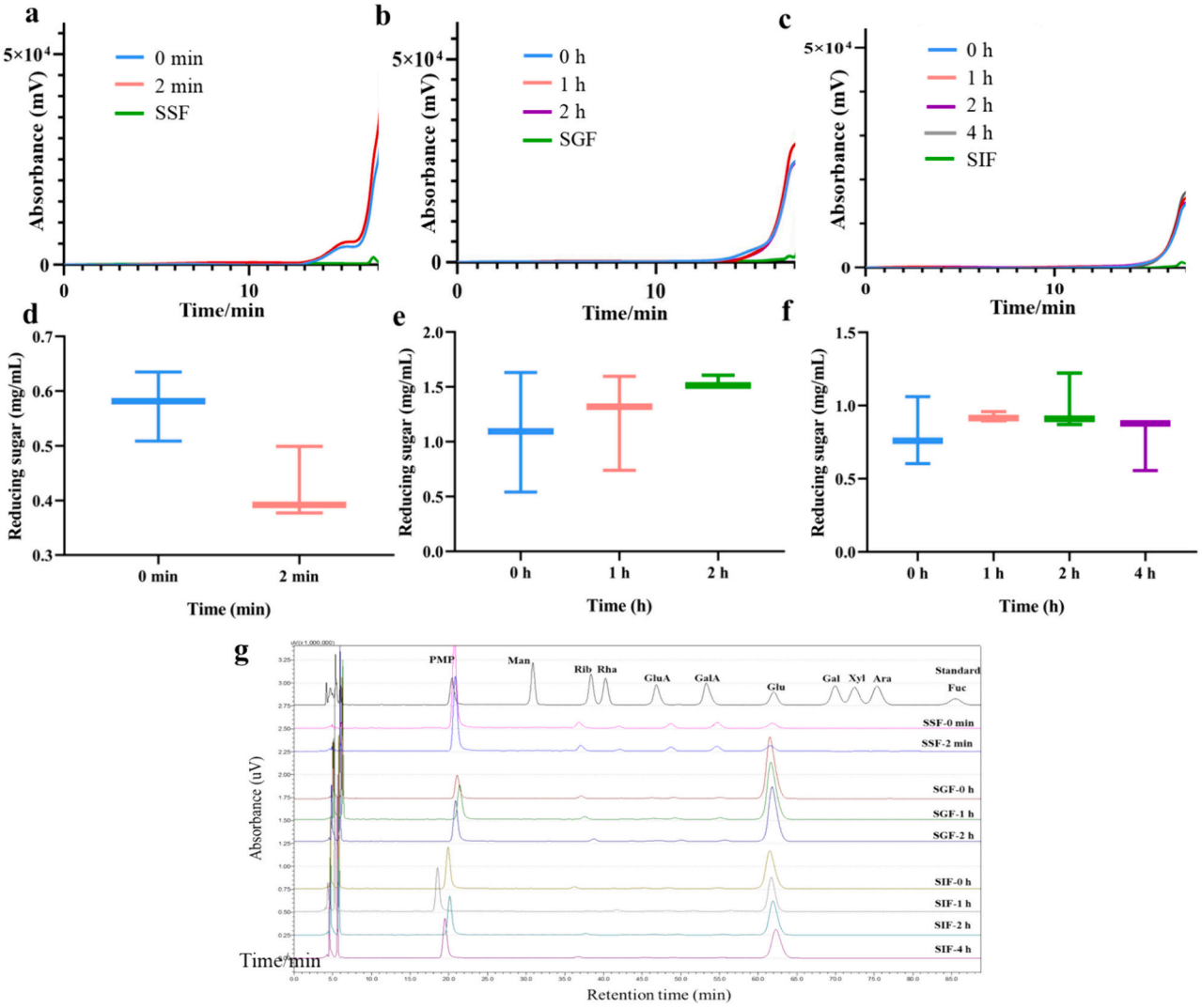


**Fig. 2.** Changes of LLP11 during simulated digestion.
$M_w$ variation of LLP11 during SSF (a), SGF (b), and SIF (c) digestion; Reducing sugar contents of LLP11 in SSF (d), SGF (e) and SIF (f) digestion; Changes of monosaccharide production during digestion (g).

($p < 0.01$), and increased Actinobacteriota ($p < 0.01$) and Firmicutes compared to the Con group. At the genus level (Fig. 3b, c), *Klebsiella* ($p < 0.01$), *Escherichia-Shigella* ($p < 0.01$), *Enterobacter* ($p < 0.01$), and *Veillonella* ($p < 0.01$) were inhibited, while the growth of *Bifidobacterium* ($p < 0.001$) *and Lactobacillus* ($p < 0.05$) were significantly enhanced after LLP11 intervention.

Consistent with the community composition results, the LDA score of LEfSe analysis (LDA > 3.5, $p < 0.05$) (Fig. S6) showed that the genera of *Bifidobacterium*, *Mitsuokella,* and *Lactobacillus* were enriched in LLP11 group, in contrast, *Klebsiella*, *Escherichi-Shigella*, *Veillonella*, *Conllinsella*, and *Catenibacterium* were enriched in the Con group. At the species level, *B. pseudocatenulatum* and *B. longum* were observed as the main strains of *Bifidobacterium*. Importantly, *Klebsiella* and *Escherichia-Shigella* are opportunistic pathogens. The commensal pathobiont *Klebsiella pneumonia* (*Klebsiella* spp.) is a common cause of pneumonia that can lead to intense lung injury correlated with infective exacerbations (Bengoechea & Sa Pessoa, 2018). Recently, evidence has highlighted the bidirectional crosslinking of gut microbiota and respiratory diseases through the gut-

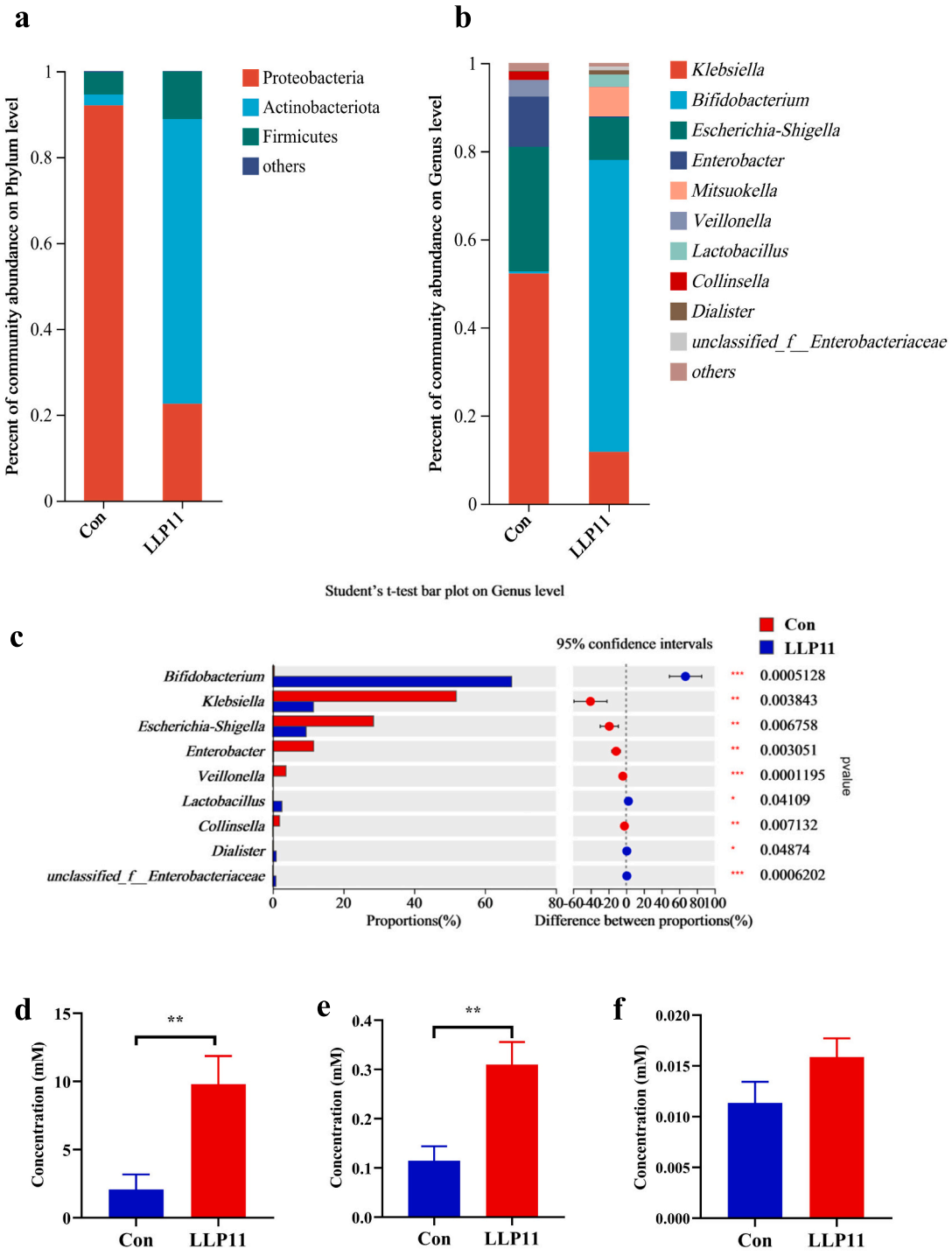


**Fig. 3.** Effects of LLP11 on the intestinal microbiota.
The relative abundance of GM at phylum level (a); The relative abundance of GM at genus level (b); Significance test for inter group differences at genus level (c); The contents of acetic acid (d), propionic acid (e) and butyric acid (f) in the fermentation broth after 24 h. ($n = 3$, $^{**}p < 0.01$).

lung axis (Mindt & Digiandomenico, 2022). *Bifidobacterium* spp. is a famous probiotic with significant therapeutic effects on relieving chronic diarrhea and constipation, as well as antioxidant and immune regulation (Dempsey & Corr, 2022). Oral administration of *B. longum* could defend against *K. pneumoniae* induced lung infection and relieve inflammation by activating the TLR-signaling pathway (Vieira et al., 2016). To some extent, our results could explain the potential mechanism of Longya lily with the traditional efficacy of relieving coughs and removing phlegm from the point of gut microbiota.

SCFAs act as anti-inflammation and immunomodulation agents by activating the G protein-coupled receptors (GPCRs) on epithelial or immune cells (Mindt & Digiandomenico, 2022). The activated immune cells can migrate from the intestine to the lung and defend against pulmonary helminth and bacterial infections (Gray et al., 2017). After 24 h fermentation with LLP11, the pH value decreased from 6.18 ± 0.02 to 4.13 ± 0.03 (Δ pH = 2.05). Additionally, the contents of acetic acid ($p < 0.01$), propionic acid ($p < 0.01$), and butyric acid were increased compared to the Con group (Fig. 3d-f).

### 3.7. Utilization of LLP11 and its effect on the growth of Bifidobacterium strains

To investigate the effect of LLP11 on the growth of *Bifidobacterium* spp., *B. pseudocatenulatum* and *B. longum* were cultured in basic nutrient medium with LLP11 (2.5, 5, and 10 mg/mL) as the sole carbon source. Compared to the BBL medium, the growth curve showed that LLP11 significantly promoted the growth of *B. longum* and *B. pseudocatenulatum* at all concentrations (Fig. 4a, b). Besides, *B. pseudocatenulatum* had a faster and higher growth compared to *B. longum*. The growth curve of LLP11 on *B. pseudocatenulatum* mixed with *B. longum* fell between those of *B. longum* and *B. pseudocatenulatum*, which meant that neither synergistic nor antagonistic action existed in *B. longum* and *B. pseudocatenulatum* (Fig. 4c). In addition, the total carbohydrates of LLP11 fermented with *B. longum* decreased by 29.58%, 31.02%, and 14.02% at 2.5, 5, and 10 mg/mL after 48 h. In comparison, LLP11 fermented with *B. pseudocatenulatum* decreased by 73.38%, 58.91%, and 49.31% at 2.5, 5, and 10 mg/mL (Fig. 5a). It seemed that *B. pseudocatenulatum* had a better capacity to utilize LLP11, which was consistent with the growth curve.

*Bifidobacterium*, involved in carbohydrate metabolism, is prevalent in mammalian intestines. Genomic analyses have demonstrated that *Bifidobacterium* can employ genetic strategies to metabolize a variety of glycans as they express a large number of genes encoded by various glycoside hydrolases (Turroni et al., 2018). However, *Bifidobacterium* strains generally prefer hydrolyzing glycans with a lower polymerization degree, especially oligosaccharides with a short-chain structure, rather than highly polymerized carbohydrates (Lei et al., 2022). The efficiency of carbohydrate utilization by *Bifidobacterium* is negatively correlated with the polymerization degree of carbohydrates (Horinouchi et al., 2021; Tabasco, Fernández De Palencia, Fontecha, Peláez, & Requena, 2014). In addition, Xiang *et. al* found that polysaccharides mainly composed of glucose and mannose had a more prominent promoting effect on *B. longum* and *B. adolescentis* compared to other polysaccharides with different monosaccharide composition, which indicated that the microbial utilization of glucan kinds was selective and *Bifidobacterium* preferred glucomannans or mannoglucans (Xiang et al., 2023).

### 3.8. Quantitative analysis of acetic acid

Acetic acid is a characteristic metabolite generated by *Bifidobacterium*. Acetic acid provides energy for the gut microbiota, and activates the G protein-coupled receptors GPR41 and GPR43 (Liu, Li, et al., 2021). Besides, acetic acid potentially improves aging-related disorders (Ma et al., 2023). Interestingly, acetate can be abundantly present in the peripheral circulation. Previous work has found that acetic acid can circulate from the gut to the lungs to activate FFAR2 to defend against *Escherichia coli*-induced lung inflammation (Peng et al., 2021). As shown in Fig. 5b, the level of acetic acid significantly increased in *B. longum* and *B. pseudocatenulatum* fermentation after 48 h. These results indicated that *B. longum and B. pseudocatenulatum* could utilize LLP11 to generate acetic acid.

## 4. Conclusion

In this study, a homogenous mannoglucan LLP11 with an $M_w$ of 12.0 kDa was purified from Longya lily by membrane ultrafiltration combined with ion exchange chromatography. LLP11 had a backbone of →4)-α-D-Glc*p*-(1 → and →4)-β-D-Man*p*-(1 → with a branch of T-α-D-Glc*p*-(1 → substituted at C-6 of →4, 6)-α-D-Glc*p*-(1→. LLP11 resisted to the simulated digestion, but interacted with GM. LLP11 inhibited *Klebsiella*, *Escherichia-Shigella*, and *Enterobacter*, yet promoting *Bifidobacterium* growth and SCFAs production. Besides, LLP11 facilitated the growth of *B. pseudocatenulatum* and *B. longum* and was utilized to produce acetic acid. These results suggested that LLP11 may be a potential prebiotic candidate benefitting the fitness of *Bifidobacterium*, which might be correlated with its traditionally medicinal effect on treating respiratory diseases. Our findings highlight that LLP11 may deserve to be explored as prebiotics for adjuvant therapy of respiratory diseases. Future work will focus on the polysaccharide utilization loci and the effect of LLP11 on gut microbiota remodeling *in vivo*.

## CRediT authorship contribution statement

**Guangjian Bai:** Conceptualization, Data curation, Investigation, Methodology, Validation, Writing – original draft. **Miaoyun Ye:** Investigation, Methodology. **Li Yu:** Investigation. **Ming Yang:** Investigation. **Yaqi Wang:** Investigation, Resources, Writing – review & editing,

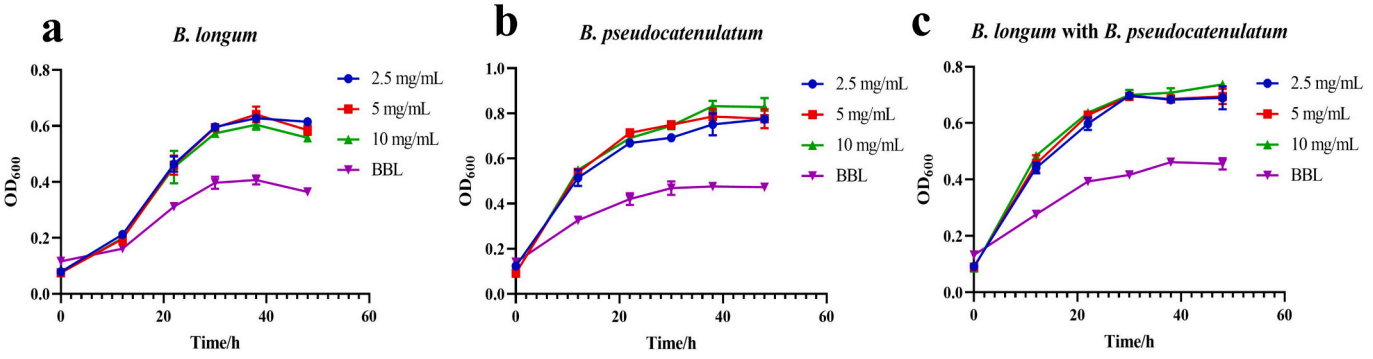


**Fig. 4.** Growth curves of two *Bifidobacterium* strains in the presence of LLP11 ($n = 3$). *B. longum* (a), *B. pseudocatenulatum* (b) and mixed *B. longum*-*B. pseudocatenulatum* (1:1) (c) was cultured in LLP11 of 2.5, 5 and 10 mg/mL and BBL medium.

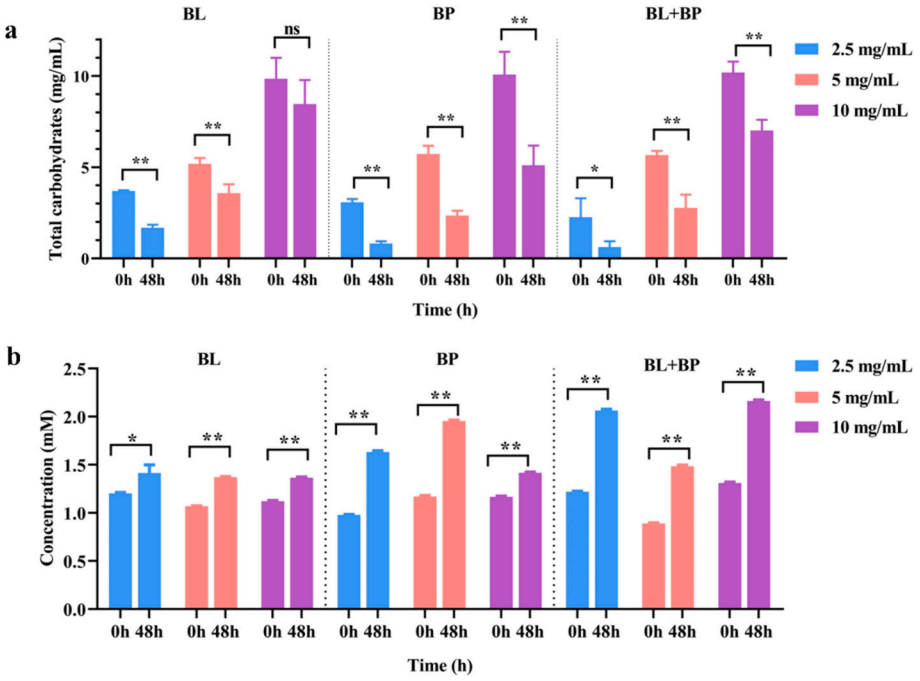


**Fig. 5.** Total carbohydrates and acetic acid content of LLP11 with *Bifidobacterium* co-cultured supernatant. Total carbohydrates (a); Acetic acid content (b) ($n = 3$, $^{*}p < 0.05$, $^{**}p < 0.01$, "ns" means not significant). Note: BL: *B. longum*; BP: *B. pseudocatenulatum*; BL + BP: mixed *B. longum-B. pseudocatenulatum* (1:1).

Funding acquisition. **Shaodan Chen:** Funding acquisition, Project administration, Supervision, Writing – review & editing.

## Declaration of competing interest

The authors declare that they have no known competing financial interests or personal relationships that could have appeared to influence the work reported in this paper.

## Data availability

Data will be made available on request.

## Acknowledgments

This work was financially supported by National Natural Science Foundation of China (82373770), Guangdong Basic and Applied Basic Research Foundation (2023A1515030151, 2023A1515012155), Open Project of Key Laboratory of Modern Preparation of TCM, Ministry of Education, Jiangxi University of Chinese Medicine (zdsys-202108) and Jiangxi Province College Students Innovation and Entrepreneurship Training Program (X202310412170).

## Appendix A. Supplementary data

Supplementary data to this article can be found online at https://doi.org/10.1016/j.fochx.2024.101671.

## References

Bai, Y., Zhou, Y., Li, X., Zhang, R., Huang, F., Fan, B., Zhang, & M.. (2023). Longan pulp polysaccharides regulate gut microbiota and metabolites to protect intestinal epithelial barrier. *Food Chemistry, 422*, Article 136225. https://doi.org/10.1016/j.foodchem.2023.136225

Bai, Y., Zhou, Y., Zhang, R., Chen, Y., Wang, F., & Zhang, M. (2023). Gut microbial fermentation promotes the intestinal anti-inflammatory activity of Chinese yam polysaccharides. *Food Chemistry, 402*, Article 134003. https://doi.org/10.1016/j.foodchem.2022.134003

Bengoechea, J. A., & Sa Pessoa, J. (2018). *Klebsiella pneumoniae* infection biology: Living to counteract host defences. *FEMS Microbiology Reviews, 43*(2), 123–144. https://doi.org/10.1093/femsre/fuy043

Chen, S., Guan, X., Yong, T., Gao, X., Xiao, C., Xie, Y., Wu, & Q.. (2022). Structural characterization and hepatoprotective activity of an acidic polysaccharide from *Ganoderma lucidum*. *Food Chemistry: X, 13*, Article 100204. https://doi.org/10.1016/j.fochx.2022.100204

Chen, Z., Zhang, D., Zhu, Q., Yang, Q., & Han, Y. (2014). Purification, preliminary characterization and *in vitro* immunomodulatory activity of tiger lily polysaccharide. *Carbohydrate Polymers, 106*, 217–222. https://doi.org/10.1016/j.carbpol.2014.02.004

Dempsey, E., & Corr, S. C. (2022). *Lactobacillus* spp. for gastrointestinal health: Current and future perspectives. *Frontiers in Immunology, 13*, Article 840245. https://doi.org/10.3389/fimmu.2022.840245

Dubois, M., Gilles, K., Hamilton, J. K., Rebers, P. A., & Smith, F. (1951). A colorimetric method for the determination of sugars. *Nature, 168*(4265), 167. https://doi.org/10.1038/168167a0

Feng, Y., Weng, H., Ling, L., Zeng, T., Zhang, Y., Chen, D., & Li, H. (2019). Modulating the gut microbiota and inflammation is involved in the effect of *Bupleurum* polysaccharides against diabetic nephropathy in mice. *International Journal of Biological Macromolecules, 132*, 1001–1011. https://doi.org/10.1016/j.ijbiomac.2019.03.242

Fu, C., Ye, K., Ma, S., Du, H., Chen, S., Liu, D., Xiao, & H.. (2023). Simulated gastrointestinal digestion and gut microbiota fermentation of polysaccharides from *Agaricus bisporus*. *Food Chemistry, 418*, Article 135849. https://doi.org/10.1016/j.foodchem.2023.135849

Gao, X., Zeng, R., Ho, C., Li, B., Chen, S., Xiao, C., Wu, & Q.. (2022). Preparation, chemical structure, and immunostimulatory activity of a water-soluble heteropolysaccharide from *Suillus granulatus* fruiting bodies. *Food Chemistry: X, 13*, Article 100211. https://doi.org/10.1016/j.fochx.2022.100211

Gray, J., Oehrle, K., Worthen, G., Alenghat, T., Whitsett, J., & Deshmukh, H. (2017). Intestinal commensal bacteria mediate lung mucosal immunity and promote resistance of newborn mice to infection. *Science Translational Medicine, 9*(376). https://doi.org/10.1126/scitranslmed.aaf9412

Horinouchi, A., Hirai, H., Hirano, R., Kurihara, S., Takagi, H., & Matsumoto, K. (2021). Intestinal immunomodulatory activity of indigestible glucan in mice and its utilization by intestinal bacteria *in vitro*. *Journal of Functional Foods, 87*, Article 104759. https://doi.org/10.1016/j.jff.2021.104759

Hou, Y., Zhao, J., Yin, J., & Nie, S. (2023). Structural properties of *Bletilla striata* polysaccharide and the synergistic gelation of polysaccharide and xanthan gum. *Food Hydrocolloids, 142*, Article 108843. https://doi.org/10.1016/j.foodhyd.2023.108843

Hui, H., Jin, H., Li, X., Yang, X., Cui, H., Xin, A., Qin, & B.. (2019). Purification, characterization and antioxidant activities of a polysaccharide from the roots of *Lilium davidii* var. *unicolor* cotton. *International Journal of Biological Macromolecules, 135*, 1208–1216. https://doi.org/10.1016/j.ijbiomac.2019.06.030

Hui, H., Li, X., Jin, H., Yang, X., Xin, A., Zhao, R., & Qin, B. (2019). Structural characterization, antioxidant and antibacterial activities of two heteropolysaccharides purified from the bulbs of *Lilium davidii* var. *unicolor* cotton.

*International Journal of Biological Macromolecules, 133*, 306–315. https://doi.org/10.1016/j.ijbiomac.2019.04.082

Lei, Y., Zhang, Y., Wang, Q., Zheng, B., Miao, S., & Lu, X. (2022). Structural characterization and *in vitro* analysis of the prebiotic activity of oligosaccharides from lotus (*Nelumbo nucifera* Gaertn.) seeds. *Food Chemistry, 388*, Article 133045. https://doi.org/10.1016/j.foodchem.2022.133045

Li, H., Wang, R., Liu, J., Zhang, Q., Li, G., Shan, Y., & Ding, S. (2020). Effects of heat-moisture and acid treatments on the structural, physicochemical, and *in vitro* digestibility properties of lily starch. *International Journal of Biological Macromolecules, 148*, 956–968. https://doi.org/10.1016/j.ijbiomac.2020.01.181

Li, W., Wang, Y., Wei, H., Zhang, Y., Guo, Z., Qiu, Y., Xie, & Z.. (2020). Structural characterization of Lanzhou lily (*Lilium davidii* var. *unicolor*) polysaccharides and determination of their associated antioxidant activity. *Journal of the Science of Food and Agriculture, 100*(15), 5603–5616. https://doi.org/10.1002/jsfa.10613

Li, X., Guo, R., Wu, X., Liu, X., Ai, L., Sheng, Y., Wu, & Y.. (2020). Dynamic digestion of tamarind seed polysaccharide: Indigestibility in gastrointestinal simulations and gut microbiota changes *in vitro*. *Carbohydrate Polymers, 239*, Article 116194. https://doi.org/10.1016/j.carbpol.2020.116194

Liu, X., Mao, B., Gu, J., Wu, J., Cui, S., Wang, G., Chen, & W.. (2021). *Blautia*-a new functional genus with potential probiotic properties? *Gut Microbes, 13*(1), 1–21. https://doi.org/10.1080/19490976.2021.1875796

Liu, Y., Li, Y., Ke, Y., Li, C., Zhang, Z., Wu, Y., Wu, & W.. (2021). *In vitro* saliva-gastrointestinal digestion and fecal fermentation of *Oudemansiella radicata* polysaccharides reveal its digestion profile and effect on the modulation of the gut microbiota. *Carbohydrate Polymers, 251*, Article 117041. https://doi.org/10.1016/j.carbpol.2020.117041

Ma, J., Liu, Z., Gao, X., Bao, Y., Hong, Y., He, X., Li, & H.. (2023). Gut microbiota remodeling improves natural aging-related disorders through *Akkermansia muciniphila* and its derived acetic acid. *Pharmacological Research, 189*, Article 106687. https://doi.org/10.1016/j.phrs.2023.106687

Mindt, B. C., & Digiandomenico, A. (2022). Microbiome modulation as a novel strategy to treat and prevent respiratory infections. *Antibiotics, 11*(4), 474. https://doi.org/10.3390/antibiotics11040474

Peng, L. Y., Shi, H. T., Tan, Y. R., Shen, S. Y., Yi, P. F., Shen, H. Q., & Fu, B. D. (2021). Baicalin inhibits APEC-induced lung injury by regulating gut microbiota and SCFA production. *Food & Function, 12*(24), 12621–12633. https://doi.org/10.1039/d1fo02407h

Song, S., Liu, X., Zhao, B., Abubaker, M. A., Huang, Y., & Zhang, J. (2021). Effects of *Lactobacillus* plantarum fermentation on the chemical structure and antioxidant activity of polysaccharides from bulbs of Lanzhou lily. *ACS Omega, 6*(44), 29839–29851. https://doi.org/10.1021/acsomega.1c04339

Tabasco, R., Fernández De Palencia, P., Fontecha, J., Peláez, C., & Requena, T. (2014). Competition mechanisms of lactic acid bacteria and bifidobacteria: Fermentative metabolism and colonization. *LWT - Food Science and Technology, 55*(2), 680–684. https://doi.org/10.1016/j.lwt.2013.10.004

Tian, J., Wang, X., Zhang, X., Chen, X., Dong, M., Rui, X., Li, & W.. (2023). Artificial simulated saliva, gastric and intestinal digestion and fermentation *in vitro* by human gut microbiota of intra polysaccharide from *Paecilomyces cicadae* TJJ1213. *Food Science and Human Wellness, 12*(2), 622–633. https://doi.org/10.1016/j.fshw.2022.07.065

Turroni, F., Milani, C., Duranti, S., Mahony, J., van Sinderen, D., & Ventura, M. (2018). Glycan utilization and cross-feeding activities by Bifidobacteria. *Trends in Microbiology, 26*(4), 339–350. https://doi.org/10.1016/j.tim.2017.10.001

Vieira, A. T., Rocha, V. M., Tavares, L., Garcia, C. C., Teixeira, M. M., Oliveira, S. C., … J. R.. (2016). Control of *Klebsiella pneumoniae* pulmonary infection and immunomodulation by oral treatment with the commensal probiotic *Bifidobacterium longum* 51A. *Microbes and Infection, 18*(3), 180–189. https://doi.org/10.1016/j.micinf.2015.10.008

Vujkovic-Cvijin, I., Sklar, J., Jiang, L., Natarajan, L., Knight, R., & Belkaid, Y. (2020). Host variables confound gut microbiota studies of human disease. *Nature, 587*(7834), 448–454. https://doi.org/10.1038/s41586-020-2881-9

Wang, F., Wang, W., Niu, X., Huang, Y., & Zhang, J. (2018). Isolation and structural characterization of a second polysaccharide from bulbs of Lanzhou lily. *Applied Biochemistry and Biotechnology, 186*(3), 535–546. https://doi.org/10.1007/s12010-018-2750-2

Wu, D., He, Y., Yuan, Q., Wang, S., Gan, R., Hu, Y., & Zou, L. (2022). Effects of molecular weight and degree of branching on microbial fermentation characteristics of okra pectic-polysaccharide and its selective impact on gut microbial composition. *Food Hydrocolloids, 132*, Article 107897. https://doi.org/10.1016/j.foodhyd.2022.107897

Xiang, Y., Cao, Y. N., Yang, S. H., Ren, Y. H., Zhao, G., Li, Q., … L. X.. (2023). Isolation and purification of *Tartary buckwheat* polysaccharides and their effect on gut microbiota. *Food Science & Nutrition, 11*(1), 408–417. https://doi.org/10.1002/fsn3.3072

Zhang, D., Liu, J., Cheng, H., Wang, H., Tan, Y., Feng, W., & Peng, C. (2022). Interactions between polysaccharides and gut microbiota: A metabolomic and microbial review. *Food Research International, 160*, Article 111653. https://doi.org/10.1016/j.foodres.2022.111653

Zhang, J., Gao, Y., Zhou, X., Hu, L., & Xie, T. (2010). Chemical characterisation of polysaccharides from *Lilium davidii*. *Natural Product Research, 24*(4), 357–369. https://doi.org/10.1080/14786410903182212

Zhang, M., Qin, H., An, R., Zhang, W., Liu, J., Yu, Q., Huang, & X.. (2022). Isolation, purification, structural characterization and antitumor activities of a polysaccharide from *Lilium davidii* var. *unicolor* cotton. *Journal of Molecular Structure, 1261*, Article 132941. https://doi.org/10.1016/j.molstruc.2022.132941

Zhou, J., An, R., & Huang, X. (2021). Genus Lilium: A review on traditional uses, phytochemistry and pharmacology. *Journal of Ethnopharmacology, 270*, Article 113852. https://doi.org/10.1016/j.jep.2021.113852

Zhu, M., Luo, J., Lv, H., & Kong, L. (2014). Determination of anti-hyperglycaemic activity in steroidal glycoside rich fraction of lily bulbs and characterization of the chemical profiles by LC-Q-TOF-MS/MS. *Journal of Functional Foods, 6*, 585–597. https://doi.org/10.1016/j.jff.2013.12.002